International Journal of Bifurcation and Chaos

DYNAMIC CELL MAPPING ALGORITHM FOR COMPUTING BASINS OF ATTRACTION IN FILIPPOV SYSTEMS

CHRISTIAN ERAZO
Department of Electrical Engineering and Information Technology,
University of Naples Federico II,
Via Claudio 21, 80125, Naples, Italy,
christian.erazoordonez@unina.it

MARTIN E. HOMER
Department of Engineering Mathematics,
University of Bristol,
Bristol BS8 1UB, UK,
martin.homer@bristol.ac.uk

PETRI T. PIIROINEN
School of Mathematics, Statistics and Applied Mathematics,
National University of Ireland, Galway,
University Road, Galway, Ireland,
petri.piiroinen@nuigalway.ie

MARIO DI BERNARDO
Department of Electrical Engineering and Information Technology,
University of Naples Federico II,
Via Claudio 21, 80125, Naples, Italy and
Department of Engineering Mathematics,
University of Bristol,
Bristol BS8 1UB, UK,
mario.dibernardo@unina.it, m.dibernardo@bristol.ac.uk

Received (to be inserted by publisher)

Discontinuities are a common feature of physical models in engineering and biological systems, e.g. stick-slip due to friction, electrical relays or gene regulatory networks. The computation of basins of attraction of such nonsmooth systems is challenging and requires special treatments, especially regarding numerical integration. In this paper we present a numerical routine for computing basins of attraction (BA) in nonsmooth systems with sliding, (so-called Filippov systems). In particular we extend the Simple Cell Mapping (SCM) method to cope with the presence of sliding solutions by exploiting an event-driven numerical integration routine specifically written for Filippov systems. Our algorithm encompasses a dynamic construction of the *cell-state-space* so that, a lower number of integration steps are required. Moreover, we incorporate an adaptive strategy of the simulation time to render more efficient the computation of basins of attraction. We illustrate the effectiveness of our algorithm by computing basins of attraction of a sliding control problem and a dry-friction oscillator.

Keywords: Filippov systems, Cell-to-Cell Mapping, Sliding motions.

1. Introduction

The dynamics of real-world systems with switching can be modeled by differential equations with discontinuities [Filippov, 1988; di Bernardo *et al.*, 2008]. Coping with the macroscopic nonsmooth events that occur in these systems poses several analytical and numerical difficulties, due to the lack of differentiability of the vector fields involved. In particular, they require a special numerical treatment during simulation [Piiroinen & Kuznetsov, 2008; Dieci & Lopez, 2009, 2012]. The computation of their basins of attraction is a very relevant problem in applications; for example, it provides useful information about complex behavior caused by friction impacts or damping, in the design of mechanical devices [Mason *et al.*, 2009; Mason & Piiroinen, 2011; Zhang *et al.*, 2015]. In the context of control theory, the problem of computing basins of attraction (or regions of asymptotic stability) in such systems is often addressed by Lyapunov methods, where regions of attraction are estimated as sublevel sets of a given Lyapunov function; see e.g. [Delpoux *et al.*, 2015; Hetel *et al.*, 2015]. However, Lyapunov methods provide conservative results meaning that the computed region is smaller than the exact basin of attraction.

Cell mapping methods (CM) provide a computationally efficient way to analyze the long term behavior of dynamical systems [Hsu, 1987]. Their key characteristic is the approximation of the continuous state space via a discrete array of cells known as *cell-state space*. Then, a cell-to-cell map is created by performing short-time integrations, from the center of each cell, to the cell which contains the endpoint of the trajectory, which completely describes the dynamics of the system. The first cell mapping method presented in the literature is the *Simple Cell Mapping* (SCM) [Hsu, 1987], which has been the basis for many cell mapping methods developed in the following years [van der Spek, 1994; Sun & Luo, 2012]. Some modifications to cell mapping methods allow the computation of basins in discontinuous systems. In [Virgin & Begley, 1999] a numerical study of an impact-friction oscillator is performed via interpolated cell mapping (ICM), where an event divergent cell is included in order to detect the grazing boundary. Other cell mapping techniques consider the switching surface, i.e. the manifold where the vector field is not differentiable, as the Poincaré mapping surface for computing basins of periodic orbits [van der Spek *et al.*, 1994; Borre & Flashner, 2011; George *et al.*, 2016]. Basins of attractions of mechanical systems have also been computed via cell mapping applications by using discrete maps instead of direct numerical integrations [Mason *et al.*, 2009; Gyebrószki & Csernák, 2014].

Fewer results using cell mapping methods have been reported in discontinuous systems with sliding solutions, mainly due to the fact that standard integration routines are inaccurate or inefficient, or both, in the region where discontinuities in the derivatives occur. For example, a possible source of numerical problems is the presence of small oscillations around the discontinuity boundary (numerical chattering) that may arise during sliding. Solutions based on smoothing the system discontinuities, e.g. by replacing a sign function with a sigmoidal one, cause the system equations to become stiff making their integration more cumbersome. Another limitation of existing algorithms based on cell-to-cell mapping is the fact that the region of interest is pre-defined by the user which implies that extra computations are required if it is desired to explore a different region of state space. In this case an adaptive extension of the state space will be more suitable to reduce the computational cost, due to the extra CM applications. In [Gyebrószki & Csernák, 2017] for example, the authors introduce an extension of the simple cell mapping method aimed at investigating different regions in the state space independently, to further, cluster them into a general mapping solution. Parallel processing capabilities of modern architectures have also been exploited within cell mapping methods, by considering different cell dimensions and several refinement stages [Kreuzer & Lagemann, 1996; Belardinelli & Lenci, 2016a]. However these techniques have not been extended, as far as we are aware, for discontinuous systems.

In order to overcome these difficulties, we introduce in this paper an algorithm, based on simple cell mapping, which exploits the event-driven integration routine proposed in [Piiroinen & Kuznetsov, 2008]. The method can automatically cope with the presence of sliding solutions, and correct for possible numerical drifts due to the high frequency switching nature of the discretization of these solutions. We incorporate

an adaptive strategy for the simulation time similar to that proposed in [Zufiria & Guttalu, 1993; Zufiria & Martínez-Marín, 2003] within the context of the *Adjoining cell mapping*, so that numerical integration is terminated once the trajectory reaches the cell which contains the endpoint of the trajectory, which drastically helps to reduce the computation time of the basins of attraction. Other cell mapping methods with non-uniform time steps have been proposed within the context of multi-objective optimization in [Crespo & Sun, 2000]. Moreover, our algorithm encompasses a method for dynamic selection of the region to be investigated, such that a lower number of integration steps are needed in contrast to the case where the region is fixed and preselected by the user. Specifically, after an initial application of SCM in a relatively small number of cells around the equilibrium or periodic solution of interest, extra layers of cells are added and examined iteratively. The mapping information is stored and used at each iteration, such that numerical integration is required starting just from the extra set of cells that were added. A similar idea within the context of the multi-objective optimization was presented in [Dellnitz *et al.*, 2005]. At the end of the process, a refinement stage making use of a subdivision technique [Dellnitz & Hohmann, 1997; Dellnitz *et al.*, 2001] is performed over the basin boundary, in order to better identify its limiting region and reduce the error due to the discretization of the state space.

Throughout the paper we illustrate the algorithm via a set of representative examples, including sliding control systems and periodically forced Filippov systems. The rest of the paper is organized as follows. In section 2 we give an overview of Filippov dynamics and introduce the concept of the simple cell mapping method. In section 3, an extension of the simple cell mapping algorithm for planar Filippov systems is presented, detailing how the grid is selected and describing the numerical integration method used for dealing with sliding motions. In section 4, we investigate the effectiveness of the algorithm, by computing the basins of attraction of a sliding control problem and a mechanical system with dry friction. Finally, we discuss advantages and disadvantages of the algorithm and possible future extensions for its improvement.

2. Background

2.1. *Filippov Systems*

The main characteristic of Filippov systems is the subdivision of their state space into disjoint subregions, wherein a smooth vector field is defined. The boundaries between different regions will be referred to as discontinuity surfaces or switching manifolds. We present a brief introduction to Filippov systems with a single discontinuity surface below; for more information and further details see e.g. [Filippov, 1988; di Bernardo *et al.*, 2008].

To begin with, we assume that the state space consists of two regions $R_1 \subset \mathbb{R}^N$ and $R_2 \subset \mathbb{R}^N$, separated by a discontinuity surface Σ defined as the zero set of a smooth scalar function $h(x) : \mathbb{R}^N \mapsto \mathbb{R}$. A bimodal Filippov system is then described as

$$\dot{x} = \begin{cases} F_1(x) & \text{for } x \in R_1, \\ F_2(x) & \text{for } x \in R_2, \end{cases} \tag{1}$$

where $F_1(x) : \mathbb{R}^N \mapsto \mathbb{R}^N$ and $F_2(x) : \mathbb{R}^N \mapsto \mathbb{R}^N$ are smooth vector fields. The regions R_1, R_2 and the surface Σ are defined as

$$R_1 = \{x \in \mathbb{R}^N : h(x) > 0\},\ R_2 = \{x \in \mathbb{R}^N : h(x) < 0\}, \tag{2}$$

$$\Sigma = \left\{x \in \mathbb{R}^N : h(x) = 0\right\}. \tag{3}$$

If the vector fields F_1 and F_2 both point towards the discontinuity surface Σ at any given point, the dynamics are assumed locally constrained to the surface, and the motion on Σ is said to be sliding. The open subset $\widehat{\Sigma} \subset \Sigma$ where the vector fields are both pointing towards Σ is often referred to as the *sliding surface*, which is attractive if it holds that [di Bernardo *et al.*, 2008]

$$\mathcal{L}_{F_1 - F_2}(h)(x) < 0, \quad x \in \widehat{\Sigma}, \tag{4}$$

and repelling if

$$\mathcal{L}_{F_1-F_2}(h)(x) > 0, \quad x \in \widehat{\Sigma}. \tag{5}$$

Here, $\mathcal{L}_{F_i}h(x) := \nabla h(x) \cdot F_i(x)$ is the *Lie derivative* of $h(x)$ with respect to the vector field F_i. Using *Utkin's equivalent control* method [Utkin, 1977], the dynamical system (1) can be extended to include the vector field on the sliding surface such that

$$\dot{x} = F_\Sigma(x), \quad \text{for} \quad \mathrm{x} \in \widehat{\Sigma}, \tag{6}$$

where

$$F_\Sigma(x) = \frac{F_1(x) + F_2(x)}{2} + \frac{F_1(x) - F_2(x)}{2}\mu(x), \tag{7}$$

and $-1 \leq \mu(x) \leq 1$. Since the motion is constrained to $\widehat{\Sigma}$, F_Σ must be tangent to $\widehat{\Sigma}$, i.e. $\mathcal{L}_{F_\Sigma}(h)(x) = 0$, which yields

$$\mu(x) = -\frac{\mathcal{L}_{F_1+F_2}(h)(x)}{\mathcal{L}_{F_1-F_2}(h)(x)}. \tag{8}$$

We can now define the sliding region as

$$\widehat{\Sigma} = \{x \in \Sigma : |\mu(x)| < 1\}, \tag{9}$$

with boundaries

$$\partial\Sigma^+ = \{x \in \Sigma : \mu(x) = 1\}, \quad \partial\Sigma^- = \{x \in \Sigma : \mu(x) = -1\}. \tag{10}$$

2.2. *Simple Cell Mapping*

In cell mapping methods, the state space of a dynamical system is restricted to a bounded region $\Omega \subset \mathbb{R}^N$ partitioned into cells, called *cell state space*. Specifically such space is given by

$$\Omega = \left\{x \in \mathbb{R}^N : x_i^{(\mathrm{l})} \leq x_i \leq x_i^{(\mathrm{u})},\ i = 1, \ldots, N\right\}, \tag{11}$$

where $x_i^{(\mathrm{l})}$ and $x_i^{(\mathrm{u})}$ indicate the lower and upper limit of each of the N state variables of the system. The partition of Ω into cuboidal cells is performed by dividing each interval $[x_i^{(\mathrm{l})}, x_i^{(\mathrm{u})}]$ into M_i intervals of equal length δ_i, that is

$$\delta_i = \frac{x_i^{(\mathrm{u})} - x_i^{(\mathrm{l})}}{M_i}, \quad i = 1, \ldots, N.$$

In this way, Ω is divided into M cuboidal cells, with

$$M = \prod_{i=1}^{N} M_i.$$

Each cell is denoted by an index $j \in 1, \ldots, M$. We describe some properties and definitions related to the simple cell mapping (SCM) which are used throughout the paper.

- *Cell*: An element of the cell state space represented by a center point and lengths along each dimension.
- *Cell index* (*index*, for short): A unique identifier for each cell.
- *Image*: A mapping from one cell to another. The mapping is obtained by integrating the system using the center point of the given cell as initial condition, until the trajectory enters into a new cell.
- *Periodic group* (PG): A set of cells that have been already processed, denoted as n-P group, where $n \in \mathbb{Z}^+$ indicates the period to which those set of cells belong. A cell belonging to an n-P group is denoted as an n-P cell.
- *Transient cell*: A cell or a set of cells that after some mapping end up into an n-P cell.
- *Adjoint cells*: Cells that have at least one corner point in common.

- *Group number*: A unique identifier for each periodic group.
- *Sink cell*: A special cell indicating that the trajectory is being mapped outside of the cell state space.

For a system described by a set of ordinary differential equations (ODEs), the mapping procedure starts by integrating the system (1) and (6) during a fixed time, using the center point of a cell as the initial condition. After that time, if the cell which the trajectory enters has not already been processed, a new trajectory is initiated from the center of the new cell. This sequence is repeated until the trajectory reaches a cell that has already been processed, indicating that an n-P cell has been found, which within SCM implies the existence of a periodic solution. This process is carried out for each regular cell belonging to the cell state space until all cells have been processed, see Fig. 1 (a) for a graphical interpretation of the mapping process.

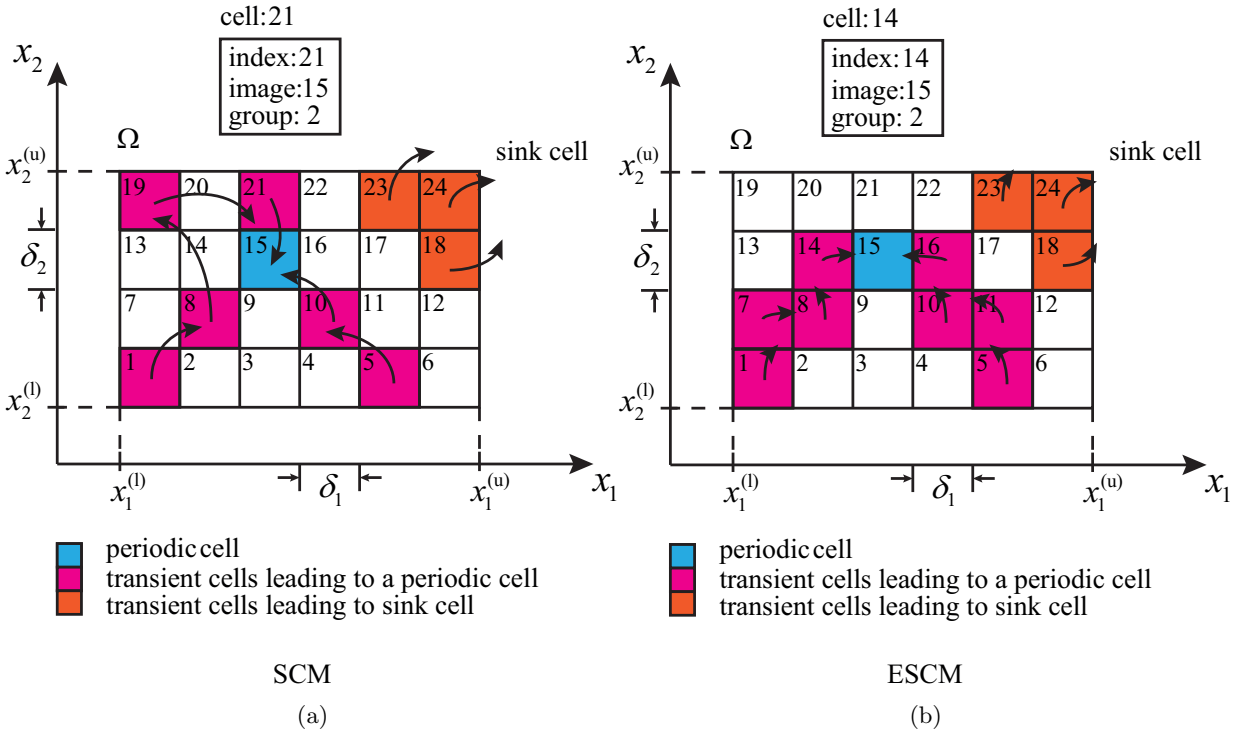

Fig. 1. Example illustrating the mapping process and some cell's properties (cell:21, cell:14) within SCM and ESCM. Two mapping processes are initialized in cells labeled with indexes 1 and 5, in both methods. Some mapping steps indicate the presence of a stable fixed point inside of the 2-P cell with index 15. Unlike the SCM (a), an adaptive strategy for the simulation time is incorporated in ESCM (b) making the integration time as lows as possible.

3. Enhanced SCM for Filippov systems

Due to the fact that existing cell mapping methods are not able to address the presence of discontinuities in Filippov systems and particularly the occurrence of sliding mode solutions, here we extend the simple cell mapping method by embedding the numerical routine to integrate bimodal Filippov systems described in [Piiroinen & Kuznetsov, 2008]. In addition, we consider the dynamic evolution of the cell state space with a refinement stage over the basin boundary cells in order to cover the basin of the region under investigation and to reduce the discretization error. Two stop integration criteria are incorporated so that, during the first stage of the algorithm, the integration is terminated as the trajectory leaves the initial cell, as shown in Fig. 4 (a). While in the refinement stage the numerical integration carried out over the cells lying on the boundary of the basins of attraction, is allowed until the trajectory reaches some cell that is not part of the basin boundary cells as shown in Fig. 4 (b). This modification along with the dynamic construction

of the state space, allow us to drastically reduce the computational cost.
Next, we describe in greater detail each of the two proposed innovations leading to an enhanced SCM for Filippov systems.

3.1. *Integration method*

Standard numerical methods for solving ODEs are based on truncation error schemes, however these methods may become inaccurate or inefficient when discontinuities occur [Dieci & Lopez, 2012]. For example, undesired behaviors such as small oscillations around Σ (numerical chattering behavior) must be properly taken into account. One strategy to solve this problem is to use event-detection routines, in which the discontinuity is considered as an event function such that when a numerical solution reaches the discontinuity surface Σ, a new vector field (the so-called sliding or Filippov vector field (6)) is constrained to evolve over Σ until certain conditions are satisfied. This event-driven scheme was successfully implemented for simulating Filippov systems for a single discontinuity surface in [Piiroinen & Kuznetsov, 2008], resulting in an automatic and robust algorithm for studying a wide variety of problems, [Dieci & Lopez, 2012; Leonov *et al.*, 2014; Burns & Piiroinen, 2015]. The event functions considered in [Piiroinen & Kuznetsov, 2008] are

$$e_1(t,x) := h(x), \quad e_2(t,x) := \mathcal{L}_{F_1}h(x), \quad e_3(t,x) := \mathcal{L}_{F_2}h(x)$$

where $e_1(t,x)$ locates intersection points between the flow and the discontinuity boundary Σ, checking the possible existence of sliding dynamics, while $e_2(t,x)$ and $e_3(t,x)$ allow to keep track the sliding flow when it enters into R_1 or R_2, respectively. A description of the tasks accomplished by the numerical routine is given below:

(i) Smooth vector fields outside of Σ, R_1 or R_2 are integrated in time by standard numerical integration routines.
(ii) Their intersection points with the discontinuity boundary are precisely located as trajectories reach Σ.
(iii) The vector field on $\widehat{\Sigma}$ is used to integrate sliding mode solutions (7) in time.
(iv) Possible numerical drifts while evolving in $\widehat{\Sigma}$ are carefully avoided by monitoring transversality conditions and by means of an appropriate numerical extension of the Filippov vector field (see [Piiroinen & Kuznetsov, 2008] for further details).
(v) While in Σ conditions are constantly monitored to decide whether to remain on the switching boundary or to leave it.

The numerical routine proposed in [Piiroinen & Kuznetsov, 2008] is mostly used for Filippov systems with a single discontinuity surface, limiting the computation of the basins of attraction for such kind of systems. Nevertheless, it is straightforward to extend the integration routine for an arbitrary number of discontinuity surfaces as discussed in [Piiroinen & Kuznetsov, 2008]. For example, in the case of biological and mechanical systems with two discontinuity surfaces where the sliding vector field at the intersection between surfaces is well-defined, the equivalent control method [Utkin, 1977] and the analytical results of the entry and exit points of co-dimension 2 sliding vector fields reported in [Dieci *et al.*, 2013] can be straightforwardly implemented for simulating accurately such systems. The main disadvantage with this approach is that the number of surfaces and event locations grow quickly with the number of discontinuity surfaces which naturally increases the simulation time.

3.1.1. *Integration stopping criterion*

One limitation of the SCM is that the integration time is global, and selected arbitrarily beforehand. This may introduces spurious mapping results when the integration time is relatively short, since the trajectory may remain within the same cell from where the simulation started instead of reaching the image cell, which under SCM will indicate erroneously the presence of a new attractor. On the other hand, if the integration time is relatively large, then the computational cost of the algorithm might become unnecessarily large.
Therefore, to avoid these limitations, we introduce two integration stop criteria to render the selection of

the simulation time adaptive. Before the refinement stage, the numerical integration is terminated only once the trajectory reaches the image cell. In particular, we introduce an extra event function in the numerical integration routine defined as

$$e_4(t,x) = \|x(t_n) - x(t_0)\|_\infty - \frac{\delta_i}{2} + \varepsilon, \tag{12}$$

where $x(t_0)$ and $x(t_n)$ denote the current initial point and the current end point of the trajectory, respectively, ε is a small positive parameter which guarantees that the trajectory has left the initial cell and $\|\cdot\|_\infty$ is the infinity vector norm. The extra event function allows to keep track the flow so that integration continues until the trajectory reaches a threshold determined by the predefined cell-width δ_i. Instead, during the refinement stage, the integration continues until the flow reaches a cell that has been already tagged in earlier iterations, provided that it is not part of the boundary cells, as shown in Fig. 4 (b).

In the flow chart in Fig. 2 we present an overview of the algorithm for simulating Filippov systems with one discontinuity surface. A description of the tasks accomplished by the numerical integration routine is given below:

Algorithm 1 A description of the numbered boxes in the flow chart in Fig 1 is given here.

1: Initialize the program with the solver properties, vector fields, IC and provide an initial simulation time $Tspan$.
2: Determine the initial state of the system, Σ, R_1 or R_2.
3: Solve the current ODE until an event e_i occurs.
4: Check if time is equal to the final time.
5: Check region of the state space in which the system is, according to the event function e_i.
6: Set the corresponding vector field F_1, F_2 or F_Σ and go to 4.

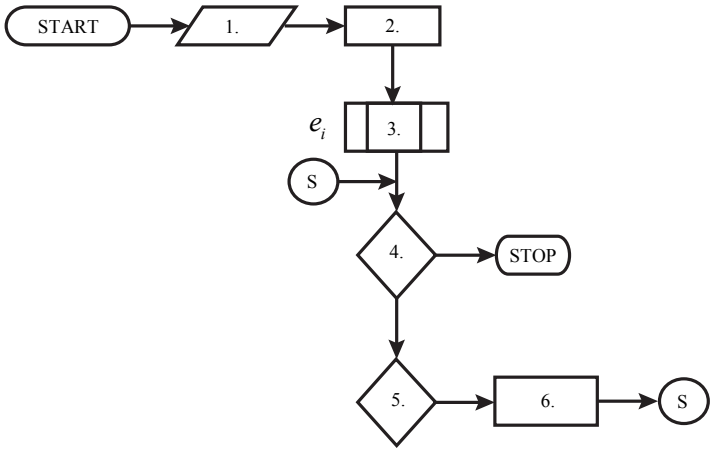

Fig. 2. A schematic flow chart of the algorithm for simulation of Filippov systems with one discontinuity surface. A description of the numbered boxes is given in Algorithm 1.

In principle, the integration time can be selected considerably big since once the trajectory has reached some cell outside of the boundary region the integration is terminated.

3.2. *Cell state space construction*

When applying the SCM, the discretization of the state space introduces some errors due to a possible inconsistency between the end point of a trajectory segment within a cell and the start of the subsequent

trajectory segment. Hsu [Hsu, 1987] claims that this problem can be solved by using a more refined grid, but this increases the computational cost of the algorithm. To overcome this problem and render our method more efficient, we adopt the idea of recovering algorithm presented in [Dellnitz *et al.*, 2005] to create a dynamically allocated cell grid, which starting from a small area contained in the basin of attraction of the attractor of interest, is grown so as to map the entire basin of attraction and isolate its boundaries. Specifically, the algorithm constructs an initial cell state space with the information provided by the user (for example a point in the phase space). Then after a first application of SCM, the algorithm automatically adds and examines layers of cells according to whether or not the cells lie in the basin of attraction. The algorithm uses information about earlier iterations such as group numbers and indexes to determine if the extra set of cells belongs to the basin of attraction. For example, when a trajectory starting in the extra set of cells enters into a cell that has been tagged as part of the basin of attraction, the extra cell is also tagged with the same periodic group and therefore tagged as belonging to the basins of attraction. A graphical representation of the stages of the algorithm is shown in Fig. 3.

It is worth nothing that the construction of the cell state space is independent of the location of the discontinuity surface. Therefore, there is no need for a special treatment of those cells that cover the switching manifold.

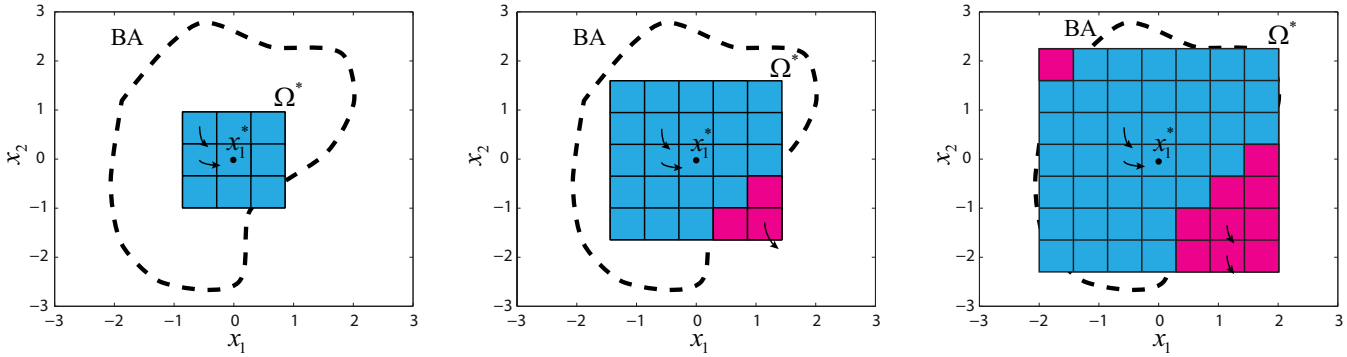

Fig. 3. Illustration of initial steps of ESCM algorithm before the refinement stage, for a fixed point x_1^*. The boundary of the basin of attraction of x_1^* is represented by the black dash line while arrows stand for trajectories mapping inside and outside of the studied region Ω^*. An initial region covering the attractor is examined by ESCM at the first step graph (a), subsequently in step 2 and 3 layers of cells are added and examined in (b) and (c).

Finally, we incorporated into the main program a sub-division routine [Dellnitz & Hohmann, 1997] to isolate and to redefine the cells that lie on the boundary of the basin of attraction. Other applications of subdivision algorithms can be found in [Schütze *et al.*, 2009; Dellnitz *et al.*, 2009; Ringkamp *et al.*, 2012] in the context of global optimization. Under the ESCM algorithm described previously, cells that are located on the boundary of two or more attractors satisfy two properties. The first is that they have different group numbers, and the second is other property is that they are adjoint, i.e., the distance between the center points of the cells is equal to the cell size δ_i. Once the boundary cells have been found, they are subdivided and investigated by applying again our enhanced SCM algorithm as shown in Fig. 4.

4. Applications

Next, we present two representative examples, to illustrate the effectiveness of our proposed algorithm. The two main stages of our algorithm, that is, the construction of the cell state space and the cell size refinement are validated by computing the domains of attraction of a sliding control

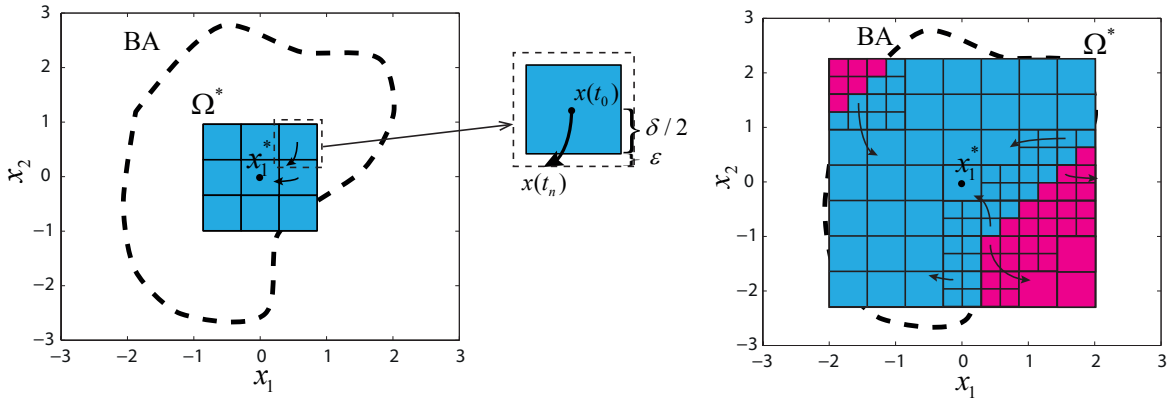

Fig. 4. Boundary refinement of the previous example. In this illustration, boundary cells are subdivided into a 4×4 grid of cells and each of which is investigated by the ESCM algorithm. Some mapping processes evidence the difference between the stop-integration criterion used in the first applications of the algorithm (a) and the one used in the refinement stage (b). In this example we assume equal partitions of the state space, i.e. $\delta = \delta_1 = \delta_2$.

problem and a dry friction oscillator. In all examples the ODE-solver `ode45` (4th-order Runge Kutta) has been used with Matlab's routines. The software used in these examples can be downloaded from `https://sites.google.com/site/dibernardogroup/download`.

4.1. *Sliding control system*

Sliding mode control is a well known nonlinear control strategy which is used in a wide range of technical domains, mainly due its simple implementation and remarkable robustness properties [Utkin *et al.*, 2009; Herbertt, 1993]. Here, we consider a second order system with a linear sliding surface. Choosing some representative parameter values, we select the closed loop system

$$\dot{x} = \begin{pmatrix} -1 & 1 \\ 0 & 3 \end{pmatrix} x + \begin{pmatrix} 0 \\ 1 \end{pmatrix} u, \tag{13}$$

where the discontinuous control is given by $u = -10\,\mathrm{sgn}(x_1 + x_2)$. The control strategy is designed to steer the system dynamics to the zero equilibrium point, which lies on the discontinuity manifold, and can therefore be classified as a pseudo-equilibrium [di Bernardo *et al.*, 2008]. Now, by adopting the formalism of Filippov systems, the vector fields corresponding to each partition of the state space can be written as

$$F_1(x) = \begin{pmatrix} -x_1 + x_2 \\ 3x_2 - 10 \end{pmatrix}, \quad F_2(x) = \begin{pmatrix} -x_1 + x_2 \\ 3x_2 + 10 \end{pmatrix}, \tag{14}$$

with the zero-level set $\Sigma_1 = \left\{x \in \mathbb{R}^2 : x_1 + x_2 = 0\right\}$ defined as the switching manifold. Straightforward investigations shows that each of the vector fields F_1 and F_2 has a hyperbolic equilibrium point and near both are of saddle-type. This gives rise to an invariant set limited by the stable manifolds of the saddle solutions, with the zero equilibrium as a fixed point.

To analyze the basin of attraction of the control system (13), we apply the ESCM. Some of the steps of the algorithm used to construct the BA of interest are shown in Fig. 5, while the final result is depicted in Fig. 6. Cells colored in blue belong to the basin of attraction of the equilibrium $x_1^* = (0, 0)$, while initial conditions in the magenta cells are mapped outside the basin of attraction. The total number of cells investigated by the ESCM at the end of the first stage is 361, as shown in Fig. 5 (f). Nevertheless, it is worth noting that, at each step of the algorithm just a small group of regular cells is investigated, since starting from a small set of cells around the origin, extra layers of cells are only added and examined iteratively. Once the entire basin has been mapped a refinement stage is performed in order to get more

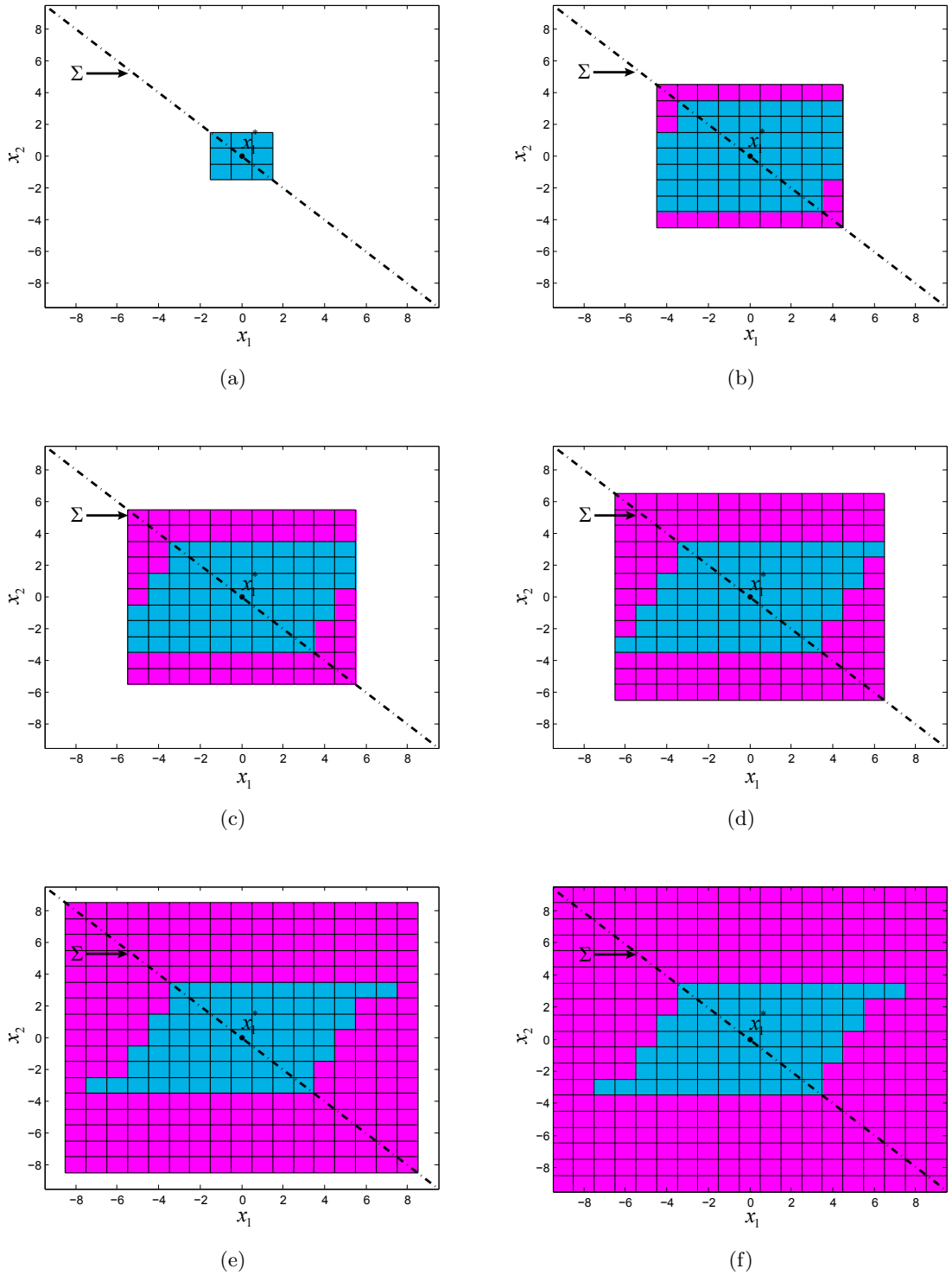

Fig. 5. Sequence of the dynamic construction of the cell state space, by assuming regular cells, i.e. $\delta = \delta_1 = \delta_2$. The black lines are used to represent the cell state space, so that each square represents a cell. The black dash-line corresponds to Σ. The initial region (blue cells) used in the first iteration is shown in (a). The 3^{nd}, 4^{th}, 5^{th} and 6^{th} iterations of the algorithm are shown in (b)-(e), respectively. A first (coarse) approximation of the basins in the 7^{th} iteration is shown in (f).

accurate results, in which the boundary cells are split, and the ESCM is applied again as described above.

Another advantage of the refinement is that the initial cell dimensions can be relatively large, so that a

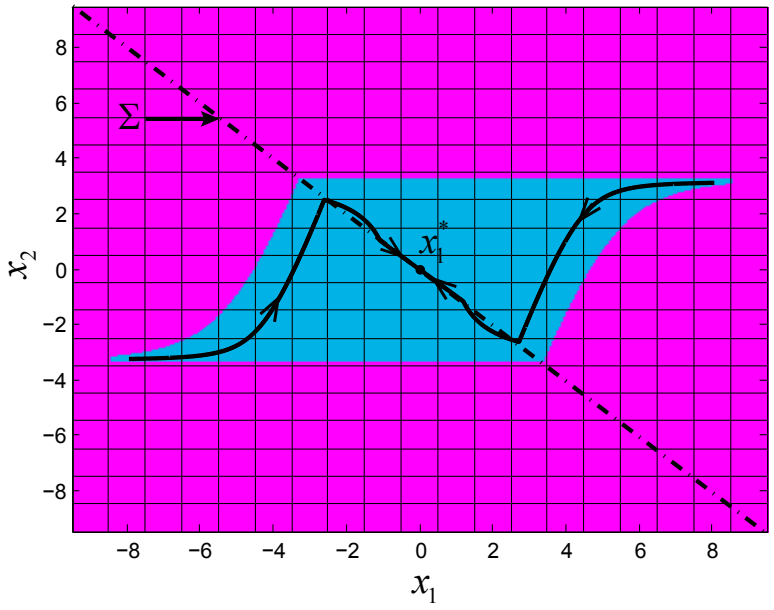

Fig. 6. Basins of attraction for the sliding control problem (13) using ESCM, for an initial resolution of 19×19 grid of cells, initial cell size of $\delta^* = 1$ (initial stages) and $\delta^{**} = 0.083$ for the refinement stage. Black curves stand for trajectories inside of BA of x_1^*, for initial conditions $(x_1, x_2) = (8, 3.3)$ and $(x_1, x_2) = (-8, -3.3)$ while the dash-line indicates the switching manifold.

bigger region of state space can be explored with a relatively lower number of iterations of the algorithm being required.

To provide a validation of the ESCM performance, in terms of the number of investigated cells and the total CPU time spent in the mapping process, the BA shown in Fig. 6 was computed using the SCM and the ESCM with fixed integration time (ESCM-Ts). The computation times and the number of investigated cells for the sliding control example (13) are shown in Table 1. The results indicate a reduction of at least 50% of the computational cost spent by the classical SCM applications, even using the ESCM with fixed integration-time. These results suggest that the strategy of combining different cell sizes and adaptive schemes of the integration times within cell mapping methods is effective not only for reducing the computational cost, but also for finding new invariant regions in Filippov systems.

Table 1. Total number of investigated cells within SCM, ESCM-Ts and ESCM. The CPU time used in all three methods is reported below.

Method	Integration time (s)	Number of cells			CPU time (s)
		$\delta^* = 1$	$\delta^{**} = 0.083$	Total	
SCM	4	0	51948	121104	1315
ESCM-Ts	4	361	13536	20713	409
ESCM	adaptive	361	13536	20713	229

It is worth nothing that, in all three cases, we set the algorithm parameters so as to obtain the same diagram shown in Fig. 6. Thus, in the case of the SCM we set a grid with the same dimension chosen in the final refinement stage of the ESCM. Thus, since we considered a grid of cells of 19×19 in the initial

stage of the algorithm (Fig. 5 (a)-(f)) and a grid of cells of 12×12 in the refinement process 12×12, we set a 228×228 grid of cells in the SCM application.

To further test the efficiency of the ECSM, we computed the same basin of attraction using the ESCM with different fixed integration times. The CPU times for different integration times are listed in Table 2, indicating that even with fixed integration time, the ESCM is superior to the classical cell mapping methods.

Table 2. Comparison of the CPU time for different values of the simulation time.

Integration time	CPU time (s)		
	SCM	ESCM-Ts	ESCM
4	1315	409	229
8	2107	633	229
16	3739	1121	229

The lack of available numerical tools for computing basins of attraction in piecewise smooth systems makes it difficult to perform a comparison of our algorithm with respect to other strategies, however it is clear that, a better approximation is achieved in terms of the proportion of the basins found, rather than those achieved by means of other more conservative methods (e.g. Lyapunov based approaches).

4.2. *Dry friction oscillator*

Dry friction is a very common phenomenon underlying many physical applications e.g. rigid bodies, pneumatic actuators, brakes and gears. Here we consider a single-degree-of-freedom nonsmooth oscillator under external excitation, which has been widely studied [di Bernardo *et al.*, 2008; Kowalczyk & Piiroinen, 2008; Jeffrey, 2014] since it exhibits complex dynamics due to its discontinuous nature. The nonsmooth mechanical system of interest is shown in Fig. 7. It is composed of a block of mass m which is supported by a belt moving with constant velocity v. The block is connected to a fixed support by a linear elastic spring of stiffness k and is subject to an external harmonic force of magnitude A and frequency ω. The origin of the position coordinate x_1 is where the spring assumes its natural length. If the block is in the stick phase

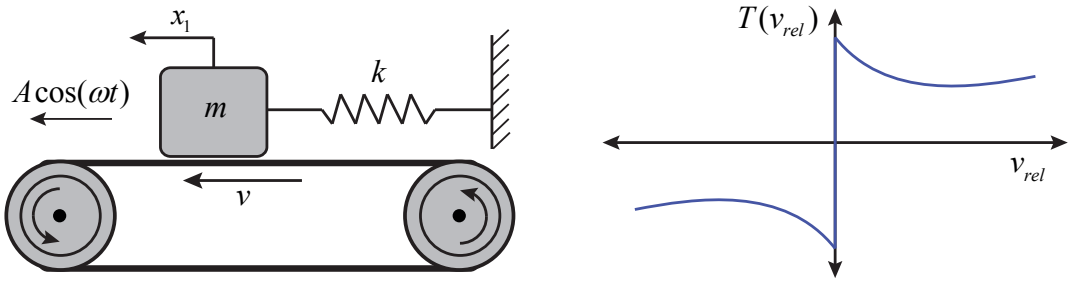

Fig. 7. The dry friction oscillator along with the adopted nonsmooth friction model, $v_{rel} = x_2 - v$.

(i.e. the block is moving at the same speed as the belt), the interaction between the spring force, applied harmonic force and friction force cause the block to start slipping (i.e. the block is moving at a different speed relative to the belt) and vice versa. The equations of motion can be expressed as

$$\begin{aligned} \dot{x}_1 &= x_2 \\ \dot{x}_2 &= -\tfrac{k}{m}x_1 + \tfrac{A}{m}\cos(\omega t) + T(x_2 - v), \end{aligned} \tag{15}$$

where x_1 and x_2 represent the position and the velocity of the block. The function $T(x_2 - v)$ describes the friction between the mass and the belt and is formulated as

$$T(x_2 - v) = \begin{cases} -g\left(\frac{\alpha}{1-\gamma(x_2-v_{dr})} + \beta + \eta(x_2 - v)^2\right) & \text{if} \quad x_2 > v, \\ g\left(\frac{\alpha}{1-\gamma(x_2-v_{dr})} + \beta + \eta(x_2 - v)^2\right) & \text{if} \quad x_2 < v. \end{cases} \tag{16}$$

It is known that for specific values of the excitation frequency ω, two stable periodic orbits and one saddle periodic orbit coexist. These periodic solutions correspond to a fixed points of the stroboscopic Poincaré map associated to the system of interest. For a detailed analysis of this system see [Merillas, 2006; Galvanetto, 2008; Colombo & Galvanetto, 2009]. By using the Filippov formalism (1), the dynamics in each partition of the state space are modeled by the vector fields

$$\begin{aligned} F_1(x) &= \begin{pmatrix} x_2 \\ \frac{-kx_1 + A\cos(\omega t)}{m} - g\left(\frac{\alpha}{1+\gamma(x_2-v)} + \beta + \eta(x_2 - v)^2\right) \end{pmatrix} \quad \text{if} \quad x_2 > v, \\ F_2(x) &= \begin{pmatrix} x_2 \\ \frac{-kx_1 + A\cos(\omega t)}{m} - g\left(\frac{\alpha}{1-\gamma(x_2-v)} + \beta + \eta(x_2 - v)^2\right) \end{pmatrix} \quad \text{if} \quad x_2 < v, \end{aligned} \tag{17}$$

with the zero-level set $\Sigma_2 = \left\{x \in \mathbb{R}^2 : x_2 - v = 0\right\}$ defined as the switching manifold. In this numerical study, we use the parameters $v = 1$, $\alpha = 0.3$, $\gamma = 1.42$, $\beta = 0.1$, $\eta = 0.01$, $A = 3.6$, $K = 1$, $g = 10$ and $\omega = 1.067$. We are interested in computing the BA for the stable periodic solutions $x_1^+ = (x_1, x_2) = (-0.685, 3.01)$ and $x_2^+ = (x_1, x_2) = (-0.295, 0.99)$). In order to use our numerical routine with periodically forced systems, it is necessary to set the integration time equal to the forcing period of the system, that is $T = 2\pi/\omega$ where ω is the excitation frequency. This effectively means that we are integrating the flow to obtain the stroboscopic Poincaré map associated to the system of interest.

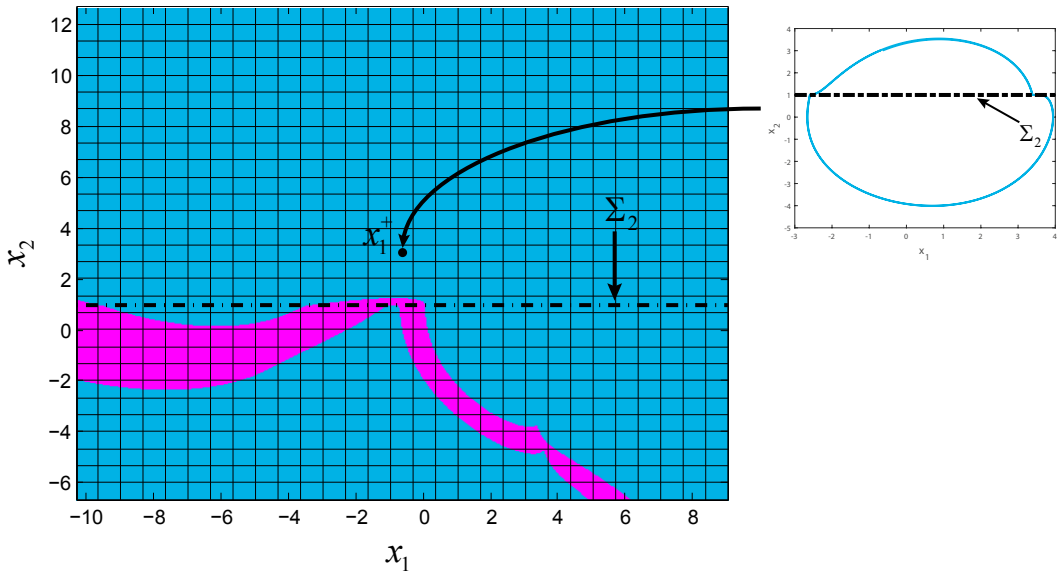

Fig. 8. Basin of attraction of the periodic solution x_1^+, for an initial resolution of 29×29 grid of cells corresponding to a cell size of $\delta^{***} = 0.66$. The cell sizes of in the refinement stage is set $\delta^{****} = 0.125$. Numerical integrations corresponding to 3 periods were performed. The numerical solution x_1^+ is shown in the right panel.

The domain of attraction diagrams of the stable periodic orbits corresponding to the fixed points x_1^+, x_2^+ and its numerical solutions are displayed in Figs. 8 and 9. The blue regions represent the set of initial

conditions for which the flow converges towards the periodic solutions x_1^+ in Fig. 8 and x_2^+ in Fig. 9, while initial conditions in the magenta region map outside of the investigated periodic solution. The computation

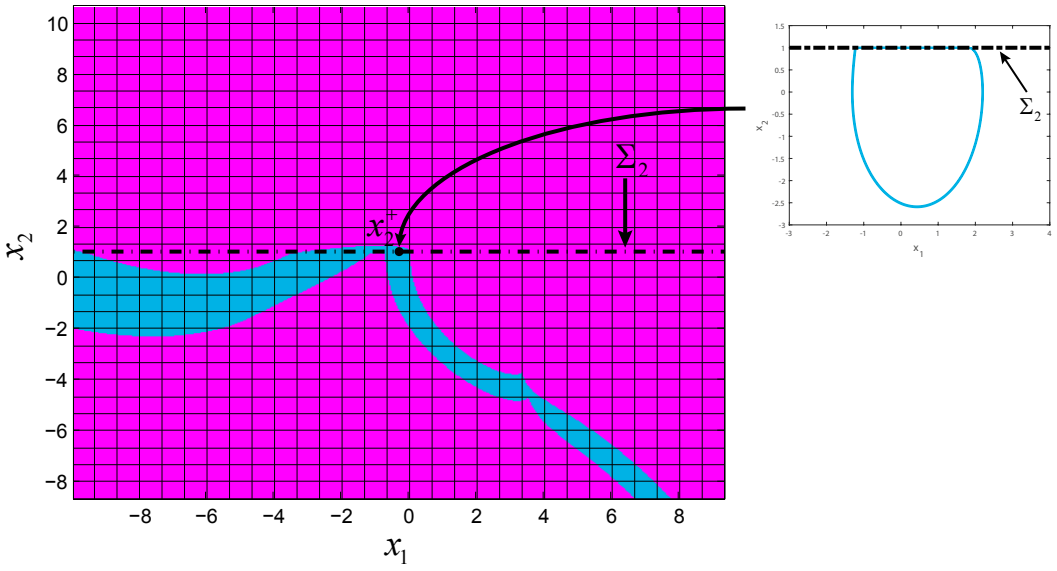

Fig. 9. Basin of attraction of the periodic solution x_2^+. The ESCM algorithm was initialized selecting a small region 3×3 grid of cells with the equilibrium point as center of the grid. Then 13 layer of cells were added and analyzed at each iteration by ESCM algorithm. In the refinement stage, each cell belonging to the boundary of the BA was divided into a 16×16 grid of cells.

of the BA reported in Fig. 8 reveals that the invariant manifold that separates the basins of attraction of x_1^+ and x_2^+ is continuous but not differentiable due to the presence of sharp corners, a phenomenon reported in the literature on PWS systems, see e.g. [Banerjee & Verghese, 2001].

Note that Figs. 8 and 9 provide essentially the same information, nevertheless, the ESCM-Ts algorithm was initialized in different regions of the state space in each case. It is worth noting that information regarding the dynamic behavior of the friction oscillator presented in this paper, is not novel; the reader is directed to [Merillas, 2006; Galvanetto, 2008] for more complete details. Rather, it is the manner in which it is computed that is new.

5. Conclusions

In this paper, we have presented a numerical routine for computing basins of attraction in bimodal Filippov systems, based on simple cell mapping. We proposed a new way to construct the cell state space in order to reduce the computational cost associated with the number of integrations performed by cell mapping methods. Another advantage is that accurate basin boundaries can be found without unnecessary computational cost through subdivision of the boundary cells. The ESCM algorithm was used for studying the BAs of a sliding control problem and a dry friction oscillator showing the stages of proposed methodology. We have shown that the computational effort of the ESCM is lower than the classic SCM with event-integration routines, even if the ESCM uses fixed simulation times. The structure of the algorithm can be easily implemented in a multi-core environment [Belardinelli & Lenci, 2016b], so that multiple analysis and subdivision processes can performed in different core processors. In the case of non planar systems the integration method used for the ESCM combined with the multidimensional cell mapping method (MDCM) [Eason & Dick, 2014; Belardinelli & Lenci, 2016a] can straightforward be integrated, to enable computation of basins of attraction in high dimensional Filippov systems. An extension of the ESCM algorithm to Filippov systems with multiple switching manifolds is directly related with the development of the integration routine as discussed in Section 3, and can be straightforwardly implemented for the case

of two switching manifolds. Nevertheless for $\widehat{M} \geq 3$ switching surfaces the situation is more involved and requires additional theoretical analysis.

References

Banerjee, S. & Verghese, G. C. [2001] "Nonlinear phenomena in power electronics: Bifurcations, chaos, control, and applications," *IEEE Press* , 73 – 85.

Belardinelli, P. & Lenci, S. [2016a] "An efficient parallel implementation of cell mapping methods for mdof systems," *Nonlinear Dynamics* **86**, 2279–2290.

Belardinelli, P. & Lenci, S. [2016b] "A first parallel programming approach in basins of attraction computation," *International Journal of Non-Linear Mechanics* **80**, 76–81.

Borre, M. & Flashner, H. [2011] "Computation of periodic solutions and their regions of attraction for flexible structures under nonlinear feedback control," *Journal of Vibration and Control* **18**, 745–756.

Burns, S. J. & Piiroinen, P. T. [2015] "A hybrid scheme for simulation of planar rigid bodies with impacts and friction using impact mappings," *International Journal of Non-Linear Mechanics* **77**, 312 – 324.

Colombo, A. & Galvanetto, U. [2009] "Stable manifolds of saddles in piecewise smooth systems," *Computer Modeling in Engineering and Sciences (CMES)* **53**, 235–254.

Crespo, L. & Sun, J. [2000] "Solution of fixed final state optimal control problems via simple cell mapping," *Nonlinear dynamics* **23**, 391–403.

Dellnitz, M., Froyland, G. & Junge, O. [2001] "The algorithms behind gaio-set oriented numerical methods for dynamical systems," *Ergodic theory, analysis, and efficient simulation of dynamical systems* **560**, 145–174.

Dellnitz, M. & Hohmann, A. [1997] "A subdivision algorithm for the computation of unstable manifolds and global attractors," *Numerische Mathematik* **75**, 293–317.

Dellnitz, M., Ober-Blöbaum, S., Post, M., Schütze, O. & Thiere, B. [2009] "A multi-objective approach to the design of low thrust space trajectories using optimal control," *Celestial Mechanics and Dynamical Astronomy* **105**, 33.

Dellnitz, M., Schütze, O. & Hestermeyer, T. [2005] "Covering pareto sets by multilevel subdivision techniques," *Journal of optimization theory and applications* **124**, 113–136.

Delpoux, R., Hetel, L. & Kruszewski, A. [2015] "Parameter-dependent relay control: Application to pmsm," *IEEE Transactions on Control Systems Technology* **23**, 1628–1637.

di Bernardo, M., Budd, C. J., Champneys, A. & Kowalczyk, P. [2008] *Piecewise-smooth Dynamical Systems Theory and Applications* (Springer Verlag).

Dieci, L., Elia, C. & Lopez, L. [2013] "A Filippov sliding vector field on an attracting co-dimension 2 discontinuity surface, and a limited loss-of-attractivity analysis," *Journal of Differential Equations* **254**, 1800–1832.

Dieci, L. & Lopez, L. [2009] "Sliding motion in Filippov differential systems: Theoretical results and a computational approach," *SIAM Journal on Numerical Analysis* **47**, 2023–2051.

Dieci, L. & Lopez, L. [2012] "A survey of numerical methods for ivps of odes with discontinuous right-hand side," *Journal of Computational and Applied Mathematics* **236**, 3967–3991.

Eason, R. P. & Dick, A. [2014] "A parallelized multi-degrees-of-freedom cell mapping method," *Nonlinear Dynamics* **77**, 467–479.

Filippov, A. F. [1988] *Differential equations with discontinuous righthand sides*, Vol. 18 (Springer Verlag).

Galvanetto, U. [2008] "Computation of the separatrix of basins of attraction in a non-smooth dynamical system," *Physica D: Nonlinear Phenomena* **237**, 2263–2271.

George, C., Virgin, L. N. & Witelski, T. [2016] "Experimental study of regular and chaotic transients in a non-smooth system," *International Journal of Non-Linear Mechanics* **81**, 55 – 64.

Gyebrószki, G. & Csernák, G. [2014] "Methods for the quick analysis of micro-chaos," **93**, 383–395.

Gyebrószki, G. & Csernák, G. [2017] "Clustered simple cell mapping: An extension to the simple cell mapping method," *Communications in Nonlinear Science and Numerical Simulation* **42**, 607 – 622.

Herbertt, S. R. [1993] "On the dynamical sliding mode control of nonlinear systems," *International journal*

of control **57**, 1039–1061.

Hetel, L., Fridman, E. & Floquet, T. [2015] "Variable structure control with generalized relays: A simple convex optimization approach," *IEEE Transactions on Automatic Control* **60**, 497–502.

Hsu, C. S. [1987] *Cell-to-cell mapping: a method of global analysis for nonlinear systems*, Vol. 64 (Springer Verlag).

Jeffrey, M. R. [2014] "Hidden dynamics in models of discontinuity and switching," *Physica D: Nonlinear Phenomena* **273**, 34–45.

Kowalczyk, P. & Piiroinen, P. [2008] "Two-parameter sliding bifurcations of periodic solutions in a dry-friction oscillator," *Physica D: Nonlinear Phenomena* **237**, 1053 – 1073.

Kreuzer, E. & Lagemann, B. [1996] "Cell mappings for multi-degree-of-freedom-systemsparallel computing in nonlinear dynamics," *Chaos, Solitons & Fractals* **7**, 1683–1691.

Leonov, G., Kuznetsov, N., Kiseleva, M., Solovyeva, E. & Zaretskiy, A. [2014] "Hidden oscillations in mathematical model of drilling system actuated by induction motor with a wound rotor," *Nonlinear Dynamics* **77**, 277–288.

Mason, J. F. & Piiroinen, P. T. [2011] "Interactions between global and grazing bifurcations in an impacting system," *Chaos: An Interdisciplinary Journal of Nonlinear Science* **21**, 013113.

Mason, J. F., Piiroinen, P. T., Wilson, R. E. & Homer, M. E. [2009] "Basins of attraction in nonsmooth models of gear rattle," *International Journal of Bifurcation and Chaos* **19**, 203–224.

Merillas, I. [2006] "Modeling and numerical study of nonsmooth dynamical systems," PhD thesis, Dept. Matematica Aplicada IV, Universitat Politecnica de Catalunya.

Piiroinen, P. T. & Kuznetsov, Y. A. [2008] "An event-driven method to simulate filippov systems with accurate computing of sliding motions," *ACM Transactions on Mathematical Software (TOMS)* **34**, 13.

Ringkamp, M., Ober-Blöbaum, S., Dellnitz, M. & Schütze, O. [2012] "Handling high-dimensional problems with multi-objective continuation methods via successive approximation of the tangent space," *Engineering Optimization* **44**, 1117–1146.

Schütze, O., Vasile, M., Junge, O., Dellnitz, M. & Izzo, D. [2009] "Designing optimal low-thrust gravity-assist trajectories using space pruning and a multi-objective approach," *Engineering Optimization* **41**, 155–181.

Sun, J.-Q. & Luo, A. C. [2012] *Global Analysis of Nonlinear Dynamics*, Vol. 2 (Springer Verlag).

Utkin, V. [1977] "Variable structure systems with sliding modes," *IEEE Transactions on Automatic Control* **22**, 212–222.

Utkin, V., Guldner, J. & Shi, J. [2009] *Sliding mode control in electro-mechanical systems*, Vol. 34 (CRC press).

van der Spek, J. [1994] "Cell mapping methods: modifications and extensions," PhD thesis, Technische Universiteit Eindhoven.

van der Spek, J., De Hoon, C., De Kraker, A. & Van Campen, D. [1994] "Application of cell mapping methods to a discontinuous dynamic system," *Nonlinear Dynamics* **6**, 87–99.

Virgin, L. & Begley, C. [1999] "Grazing bifurcations and basins of attraction in an impact-friction oscillator," *Physica D: Nonlinear Phenomena* **130**, 43 – 57.

Zhang, H., Zhang, Y. & Luo, G. [2015] "Basins of coexisting multi-dimensional tori in a vibro-impact system," *Nonlinear Dynamics* **79**, 2177–2185.

Zufiria, P. & Guttalu, R. [1993] "The adjoining cell mapping and its recursive unraveling, part i: Description of adaptive and recursive algorithms," *Nonlinear Dynamics* **4**, 207–226.

Zufiria, P. & Martínez-Marín, T. [2003] "Improved optimal control methods based upon the adjoining cell mapping technique," *Journal of Optimization Theory and Applications* **118**, 657–680.